Impact of Mg content on native point defects in $Mg_xZn_{1-x}O$ ($0 \leq x \leq 0.56$)

J. Perkins,[1] G. M. Foster,[1] M. Myer,[2] S. Mehra,[2] J. M. Chauveau,[3,4] A. Hierro,[5] A. Redondo-Cubero,[6] W. Windl,[7] and L. J. Brillson[1,8,9,a]
[1]*Department of Physics, The Ohio State University, 191 West Woodruff Ave., Columbus, Ohio 43210, USA*
[2]*Columbus School for Girls, 56 S. Columbia Ave., Columbus, Ohio 43209, USA*
[3]*Centre de Recherche sur l'Hetero-Epitaxie et ses Applications, Centre National de la Recherche Scientifique (CRHEA-CNRS), Rue B. Gregory, F-06560 Valbonne Sophia Antipolis, France*
[4]*University of Nice Sophia Antipolis, Parc Valrose, F-06102 Nice Cedex 2, France*
[5]*Dpto. Ingeniería Electrónica and ISOM, Universidad Politécnica de Madrid, Ciudad Universitaria s/n, 28040 Madrid, Spain*
[6]*Dpto. Física Aplicada y Centro de Micro-Análisis de Materiales, Universidad Autónoma de Madrid, 28049 Madrid, Spain*
[7]*Department of Materials Science and Engineering, The Ohio State University, 2041 College Road N., Columbus, Ohio 43210, USA*
[8]*Department of Electrical and Computer Engineering, The Ohio State University, 2015 Neil Avenue, Columbus, Ohio 43210-1272, USA*
[9]*Center for Materials Research, The Ohio State University, Columbus, Ohio 43210, USA*

(Received 30 January 2015; accepted 6 March 2015; published online 30 March 2015)

We used depth-resolved cathodoluminescence spectroscopy and surface photovoltage spectroscopy to measure the densities, energy levels, and spatial distributions of zinc/magnesium cation and oxygen vacancies in isostructural, single-phase, non-polar $Mg_xZn_{1-x}O$ alloys over a wide ($0 \leq x \leq 0.56$) range. Within this wide range, both defect types exhibit strong Mg content-dependent surface segregation and pronounced bulk density minima corresponding to unit cell volume minima, which can inhibit defect formation due to electrostatic repulsion. Mg in ZnO significantly reduces native defect densities and their non-polar surface segregation, both major factors in carrier transport and doping of these oxide semiconductors. [http://dx.doi.org/10.1063/1.4915491]

ZnO is a prime candidate for next generation opto- and microelectronics with a large exciton binding energy that permits efficient light emission at room temperature.[1–3] The 3.37 eV band gap of ZnO can be tuned by incorporating either Mg or Cd[4] to enable complex heterostructures that can enhance transport properties in ZnO based transistors[5,6] and optoelectronic efficiency of UV lasers,[7] light emitting diodes, and solar blind detectors.[8] The ZnO band gap increases with Mg alloying and Mg can be incorporated into ZnO at low concentrations without significantly disrupting the wurtzite structure.[7] Thus, (Mg,Zn)O layers can be stacked on ZnO layers with only a small lattice mismatch allowing for high quality heterostructures and devices.[9–11] However, ZnO occurs naturally in a zincblende or wurtzite structure, while MgO occurs naturally in a rocksalt structure, and little study has been directed at the detection and characterization of defects in the (Mg,Zn)O alloys, especially with high quality, isostructural single crystals across a wide alloy range.

The two most thermodynamically stable defects in ZnO are oxygen vacancies (V_O) and zinc vacancies (V_{Zn}), particularly under our Zn-rich growth conditions.[12] (Details of our growth conditions and defect thermodynamic stability are reported in Ref. 13.). These native point defects can be electrically charged and can contribute to free carrier densities.[14–17] Thus, V_{Zn} defects act as

[a]Email: brillson.1@osu.edu

acceptors to partially compensate degenerate carrier densities in Ga-doped ZnO.[18] Similarly, defect complexes associated with V_O can be associated with increased n-type doping in ZnO.[19] These vacancies appear to be mobile since depth-resolved cathodoluminescence spectroscopy (DRCLS) reveals pronounced segregation of V_O[20,21] and cation vacancies V_C, either V_{Zn} or V_{Mg} (this paper). Besides doping, defect levels deep within the band gap of ZnO and (Mg,Zn)O represent traps that increase "non-radiative" recombination of free carriers for transport and optoelectronic applications as well as introduce interface states that affect Schottky barrier heights. Indeed, while (Mg,Zn)O alloys are envisioned as lattice-matched confinement layers for ZnO quantum well lasers, deep level defects would degrade such lasing as well as alter the heterojunction band offsets that determine quantum well depths. Here, we describe the spatial distributions, densities, and energy levels of V_C and V_O defects and their dependence on Mg alloy composition. These defects produce energy levels deep within the (Mg,Zn)O band gap that produce nearly all midgap luminescence intensity, reflecting their recombination velocities relative to band-to-band recombination and, in turn, the impact of these native point defects on transport and light emission efficiency.

We performed these studies using a wide ($0 \leq x \leq 0.56$) range of single crystal $Mg_xZn_{1-x}O$ alloy compositions grown on *r*-plane sapphire by molecular beam epitaxy (MBE). This wide range is particularly useful in identifying electronic trends that would not be evident over a more limited range. Furthermore, X-ray diffraction (XRD) shows these *a*-face (Mg,Zn)O alloys are isostructural and single-phase over this range,[22] notwithstanding the Mg-rich lattice transformation from wurtzite to cubic rocksalt crystal symmetry. The depth dependence of defect densities measured for these alloys provided additional advantages: (1) the magnitude of defect segregation to the free surface vs. alloy composition and (2) the bulk defect densities independent of that surface segregation. A combination of depth-dependent and lattice structural techniques over this extended alloy series revealed that native defect densities rather than piezoelectric fields play a role in their near-surface segregation, that Mg in ZnO dramatically reduces native defect densities, that these defect densities depend sensitively on variations in (Mg,Zn)O alloy lattice dimensions, and that the electrostatic energy associated with surfaces and lattice unit cell dimensions can be a key factor in carrier transport and doping of these oxide semiconductors.

We grew five 1 μm thick $Mg_xZn_{1-x}O$ films with varying Mg concentration on *r*-plane sapphire. Alloy compositions measured directly from Rutherford backscattering spectrometry (RBS) were x = 0, 0.31, 0.44, 0.52, and 0.56. Using ion channeling experiments (RBS/C), we determined that ~93% of all Mg incorporated homogeneously in the epilayers occupied Zn sites in the wurtzite structure. XRD showed these films to be single phase, high quality, all with the wurtzite structure and with no cubic inclusions.[22] Atomic force microscopy (AFM) showed these surfaces to be smooth on a nanometer scale with no surface asperities. We performed DRCLS measurements using incident electron beam energies E_B = 0.1–5 keV from a glancing electron gun in an ultrahigh vacuum (UHV) system with an optical train consisting of a CaF_2 focusing lens, a sapphire viewport, and *f*-number matcher coupled to an Oriel monochromator and a CCD detector. DRCL spectra in this energy range display near band edge (NBE) and band-to-defect level transitions with nanometer depth resolution.[23–25] Depth dependence of electron-hole excitation was modeled using Monte Carlo simulations.[26] For E_B = 1, 2, 3, 4, and 5 keV, excitation peaks at depths U_0 = 7, 18, 32, 50, and 72 nm, respectively, with Bohr-Bethe maximum range $R_B \sim 3x$ longer.[13] Surface photovoltage spectroscopy (SPS) features display the onsets of photostimulated population and depopulation transitions into and out of states within the semiconductor band gap.[27–29] The increase or decrease in work function measured using an atomic force microscope in Kelvin Probe Force Microscopy (KPFM) mode[13] indicates the valence (E_V) or conduction (E_C) band nature, respectively, of such transitions and hence their energy level position within the bandgap. All these measurements were compared with deep level optical spectroscopy (DLOS), current-voltage (I-V), Schottky barrier, and steady state photo-capacitance (SSPC) measurements obtained previously on the same specimens.[30]

Figures 1(a)–1(e) show representative DRCL spectra for all five Mg concentration samples. In each spectrum, the NBE peaks at ≥3.33 eV are the dominant features, increasing in energy with increasing Mg%. Below the NBE are emissions corresponding to defect levels within the band gaps. We subtracted out the second-order replicas of the NBE peak to avoid overlap with defect features. Deep level emission intensities are normalized by NBE intensity to factor out possible variations in

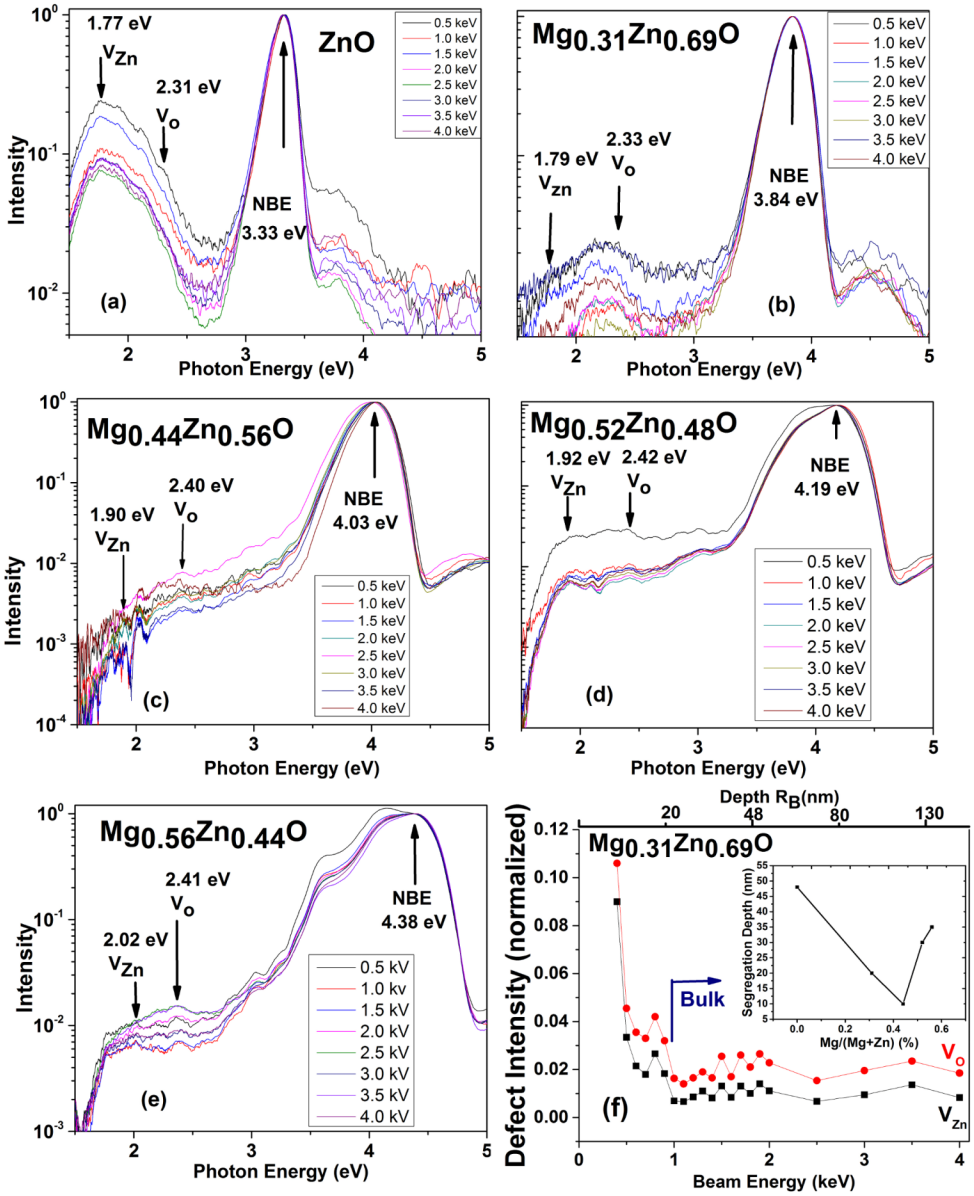

FIG. 1. (a)–(e) DRCL spectra of $Mg_xZn_{1-x}O$ for x = 0, 0.31, 0.44, 0.52, and 0.56 and E_B = 0.5–4 keV. NBE peak energies increase with Mg, while NBE-normalized deep level emission intensities decrease to a minimum at x = 0.44. (f) Representative segregation profile and bulk threshold for $Mg_{0.31}Zn_{0.69}O$ and bulk threshold versus Mg% for all samples.

collection efficiency. Normalized spectra of Figure 1 display orders-of-magnitude change in defect intensity versus Mg content. Comparison of the ZnO deep level emission to the NBE emission intensities in Fig. 1(a) shows that the 1.77 eV V_{Zn} intensity is approximately 10x lower than the NBE peak intensity. V_{Zn} clustering broadens this energy from 1.7 to 2.0 eV with increasing cluster size.[31,32] With the addition of 31% Mg in Fig. 1(b), this V_C intensity drops by nearly an order of magnitude. Similarly, V_O intensity decreases to 0.01x of the NBE intensity. Both reach minima for 44% Mg (Fig. 1(c)), then rise gradually for 52% (Fig. 1(d)) and 56% (Fig. 1(e)). Similar defect intensity decreases are evident in MgZnO grown by vapor transport but over a much smaller alloy range.[33,34] NBE energies in Fig. 1 increase linearly with Mg content up to x = 0.52, consistent with theory[35] and other reports,[36–38] deviating upward for x = 0.56, near the crossover from wurtzite to rocksalt structure.[13] Figure 1(f) presents characteristic V_C and V_O intensity profiles with depth showing strong defect segregation toward the surface over tens of nanometers with a minimum at 44% Mg (inset).

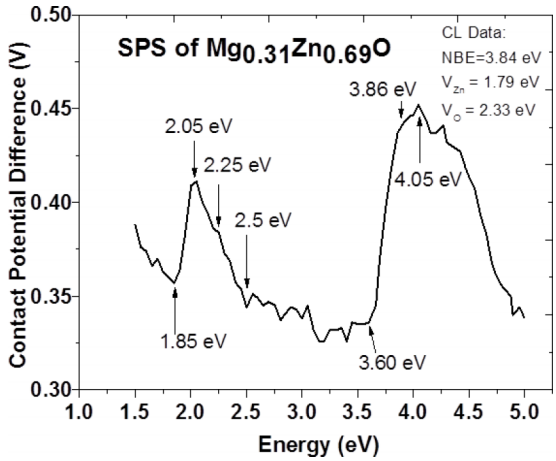

FIG. 2. SPS cpd vs. incident photon energy for $Mg_{0.31}Zn_{0.69}O$ showing changes in slope at onsets of photo-population and depopulation.

SPS spectra provided defect level positions in the bandgap for each of the alloys. The contact potential (cpd), i.e., work function difference between the reference AFM probe tip and the (Mg,Zn)O surface, indicates how the Fermi level E_F varies with photo-induced population or depopulation of states and thereby band bending within the surface space charge region. For a representative x = 0.31 spectrum in Figure 2, onsets of photostimulated depopulation (n-type positive slope change) from a gap state to E_C are evident at 1.85 and 2.5 eV, as with the 3.6–4 eV NBE transition, above which additional free carriers decrease band bending. Population transitions from E_V into a gap state (n-type negative slope change) are evident at 2.05 and 2.25 eV. Since their sum nearly equals the bandgap, the 1.85 and 2.05 eV features correspond, respectively, to photo-depopulation and population of the same gap state. Slope changes at 3.6 and 3.86 eV indicate two additional states. Five similar features are evident for all samples, in reasonable agreement with the transition energies of five DLOS trap states reported previously.[30]

Figure 3 shows band gap position of the dominant defect transitions. Here, the ZnO E_C is taken as 4.6 eV below the vacuum level, consistent with the electron affinity of the ZnO $(10\bar{1}0)$ surface,[39] and E_C (E_V) increases (decreases) with Mg% following a 2/3-1/3 rule. As Mg content varies, the defect associated with the 2.3 eV ZnO V_O level moves nearly parallel with E_V, while the 1.77 eV V_C level in ZnO tracks with E_C. These movements are consistent with their orbital—derived character, i.e., the O 2p-derived E_V maximum and the Zn 4s-derived E_C minimum.

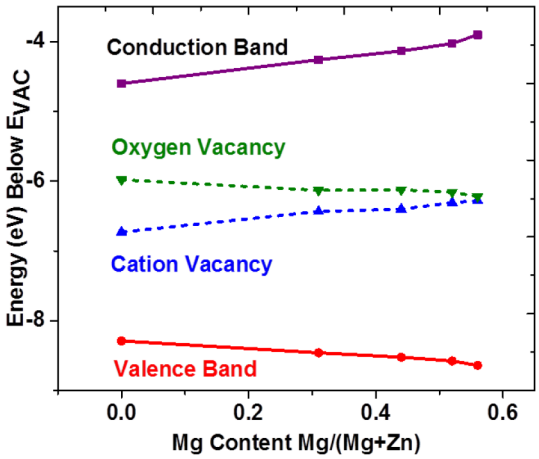

FIG. 3. SPS-derived energy levels of V_C and V_O within the (Mg,Zn)O band gap vs. Mg content. These midgap V_O (V_C) states appear to vary with valence (conduction) bands.

Figure 4 shows defect densities vs. composition and comparison with lattice constant variation. In Fig. 4(a), both V_C and V_O defect intensities I(V_C) and I(V_O) are normalized to the NBE intensity I(NBE) vs. Mg alloy content. We used DRCL spectra at 2 keV in order to avoid the near-surface segregated defects, which could increase defect intensities by more than an order of magnitude. Both I(V_C)/I(NBE) and I(V_O)/I(NBE) exhibit clear minima at x ~ 0.44. I(V_C)/I(NBE) decreases by >100x, while I(V_O)/I(NBE) decreases by >30x. Intensity differences measured from two points on the same surface correspond to <10% for x = 0 and <1% for x > 0. Trap state densities measured by *t*-SPS correlate with DRCLS intensities and display relatively good agreement[40] with Gür *et al.* DLOS results,[30] as expected from previous DLOS/*t*-SPS comparisons.[41,42] Total DLOS deep level concentrations for x = 0%, 31%, 44%, 52%, and 56% of 50.6, 6.1, 6.8, 7.8, and 5.4×10^{16} cm^{-3}, respectively,[30] also correlate with Figure 4(a). The bulk I(V_C)/I(NBE) values for ZnO are consistent with positron annihilation spectroscopy (PAS) calibration values corresponding to ~0.08×10^{17} cm^{-3} in the bulk and 0.25×10^{17} cm^{-3} at the surface.[31] Previous electrical measurements on these samples also displayed pronounced Schottky barrier decreases and sheet resistance increases above this Mg%,[30] consistent with additional donors. Figure 4(b) shows the XRD-measured variation in (Mg,Zn)O lattice parameter vs. Mg content measured by RBS. Both *a*-lattice and *c*-lattice parameters exhibit pronounced minima at x ~ 0.52.[9] A smaller range of alloy composition would not have revealed these XRD and DRCLS minima.

Both electrostatic and thermodynamic factors may contribute to the decrease in V_C and V_O defect densities with unit cell volume. Electrostatic repulsion may contribute to the free energy associated with defect formation. Thus, V_O sites in ZnO result in neighboring Zn atoms with extra charge that would otherwise lead to lattice expansion. Reduction of the unit cell dimension should increase the energy required to form such defects, lowering their density. Analogous effects are reported for native point defects in complex oxides.[43,44] The strong decrease in V_C density with Mg content may also be thermodynamically driven given the higher bond strength of MgO vs. ZnO, i.e., $-\Delta H_{298}$ (kJ/mol) = 601.6 (MgO) vs. 350.5 (ZnO). Since Mg is energetically more favorable than Zn in filling vacant Zn sites during growth, increasing Mg content would promote decreasing V_C density. Density functional theory calculations based on the pressure dependence of defect formation energies are also consistent with the defect density variations in Figure 4(a).[45]

These results show that Mg in MBE-grown *a*-plane ZnO strongly reduces V_{Zn} and V_O native point defects, which are mid-gap defects that dominate recombination and follow band edges. Nearly, the same minima of V_{Zn} and V_O defect densities in (Mg,Zn)O coincide with minima of their unit cell volumes. This correlation is consistent with the effect of these Zn and O vacancies to increase lattice electrostatic repulsion, thereby increasing formation energies and decreasing their densities. This work reveals a coupling between electronic defect and lattice structural changes and shows that the free energy associated with surfaces, interfaces, and lattice unit cell dimension can be a major factor in carrier transport and doping of these oxide semiconductors.

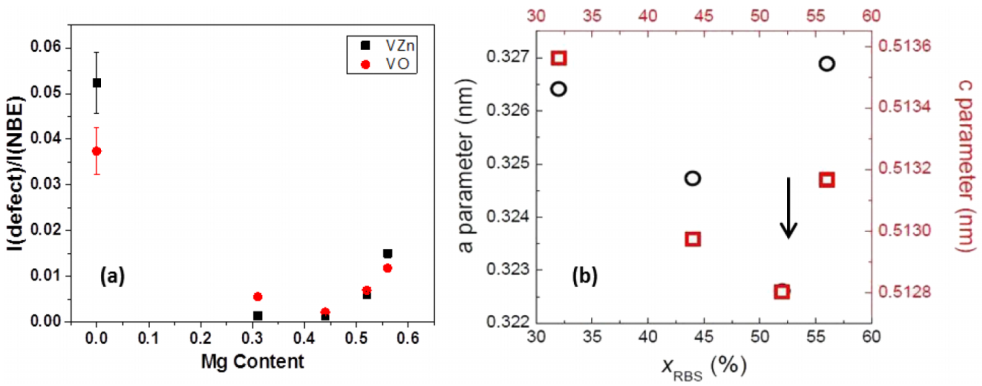

FIG. 4. V_C and V_O defect emission intensities (a) and lattice parameters (b) vs. Mg content. Point-to-point DRCLS variations signified by error bars are smaller than symbols for x > 0.

The authors gratefully acknowledge National Science Foundation, Grant No. DMR-1305193 (Charles Ying and Haiyan Wang), for support of this work. W.W. acknowledges partial funding from the Center for Emergent Materials, an NSF MRSEC (DMR 1420451) and AFOSR, Award # FA9550-14-1-0322. A.R.-C. acknowledges Juan de la Cierva program under Contract No. JCI-2012-14509 (Spain).

[1] K. Hummer, Phys. Status Solidi B **56**, 249 (1973).
[2] D. C. Look, Mater. Sci. Eng.: B **80**, 383 (2001).
[3] S. J. Pearton, D. P. Norton, L. Ip, Y. W. Heo, and T. Steiner, Prog. Mat. Sci. **50**, 293 (2005).
[4] Ü. Özgür, Y. I. Alivov, L. A. Teke, M. A. Reshchikov, S. Doğan, V. Avrutin, S. J. Cho, and H. Morkoç, J. Appl. Phys. **98**, 041301 (2005).
[5] K. Koike, K. Hama, I. Nakashima, G.-Y. Takada, M. Ozaki, K.-I. Ogata, S. Sasa, M. Inoue, and M. Yano, Jpn. J. Appl. Phys., Part 1 **43**(10B), L1372 (2004).
[6] S. Sasa, T. Maitani, Y. Furuya, T. Amano, K. Koike, M. Yano, and M. Inoue, Phys. Status Solidi A **208**, 449 (2011).
[7] A. Ohtomo, K. Tamura, M. Kawasaki, T. Makino, Y. Segawa, Z. K. Tang, G. K. L. Wong, Y. Matsumoto, and H. Koinuma, Appl. Phys. Lett. **77**, 2204 (2000).
[8] P. Tao, Q. Feng, J. Jiang, H. Zhao, R. Xu, S. Liu, M. Li, J. Sun, and Z. Song, Chem. Phys. Lett. **522**, 92 (2012).
[9] J.-M. Chauveau, J. Vives, J. Zuniga-Perez, M. Laügt, M. Teisseire, C. Deparis, C. Morhain, and B. Vinter, Appl. Phys. Lett. **93**, 231911 (2008).
[10] P. Muret, D. Tainoff, C. Morhain, and J.-M. Chauveau, Appl. Phys. Lett. **101**, 122104 (2012).
[11] G. Tabares, A. Hierro, B. Vinter, and J.-M. Chauveau, Appl. Phys. Lett. **99**, 071108 (2011).
[12] A. Janotti and C. G. Van de walle, Rep. Prog. Phys. **72**, 126501 (2009).
[13] See supplementary material at http://dx.doi.org/10.1063/1.4915491 for MBE growth conditions and reproducibility, defect thermodynamic stability, DRCLS and SPS experimental conditions, and band gap variation.
[14] L. J. Brillson, H. L. Mosbacker, M. J. Hetzer, Y. Strzhemechny, G. H. Jessen, D. C. Look, G. Cantwell, J. Zhang, and J. J. Song, Appl. Phys. Lett. **90**, 102116 (2007).
[15] Y. Dong, Z.-Q. Fang, D. C. Look, G. Cantwell, J. Zhang, J. J. Song, and L. J. Brillson, Appl. Phys. Lett. **93**, 072111 (2008).
[16] L. J. Brillson and Y. Lu, J. Appl. Phys. **109**, 121301 (2011).
[17] L. J. Brillson, Y. Dong, F. Tuomisto, B. G. Svensson, A. Y. Kuznetsov, D. Doutt, H. L. Mosbacker, G. Cantwell, J. Zhang, J. J. Song, Z.-Q. Fang, and D. C. Look, J. Vac. Sci. Technol., B **30**, 050801 (2012).
[18] D. C. Look, K. D. Leedy, L. Vines, B. G. Svensson, A. Zubiaga, F. Tuomisto, D. R. Doutt, and L. J. Brillson, Phys. Rev. B **84**, 115202 (2011).
[19] K. Vanheusden, C. H. Seager, W. L. Warren, D. R. Tallant, and J. A. Voigt, Appl. Phys. Lett. **68**, 403 (1996).
[20] H. L. Mosbacker, Y. M. Strzhemechny, B. D. White, P. E. Smith, D. C. Look, D. C. Reynolds, C. W. Litton, and L. J. Brillson, Appl. Phys. Lett. **87**, 012102 (2005).
[21] L. J. Brillson, Y. Dong, D. Doutt, D. C. Look, and Z.-Q. Fang, Physica B **404**, 4768 (2009).
[22] A. Redondo-Cubero, A. Hierro, J.-M. Chauveau, K. Lorenz, G. Tabares, N. Franco, E. Alves, and E. Muñoz, CrystEngComm **14**, 1637 (2012).
[23] L. J. Brillson, J. Vac. Sci. Technol. A **6**, 1437 (1988).
[24] L. J. Brillson, J. Vac. Sci. Technol. B **19**, 1762-1768 (2001).
[25] L. J. Brillson, J. Phys. D: Appl. Phys. **45**, 183001 (2012).
[26] P. Hovington, D. Drouin, and R. Gauvin, Scanning **19**, 1 (1997).
[27] C. L. Balestra, J. Lagowski, and H. C. Gatos, Surf. Sci. **26**, 317 (1971).
[28] H. C. Gatos and J. Lagowski, J. Vac. Sci. Technol. **10**, 130 (1973).
[29] L. Kronik and Y. Shapira, Surf. Sci. Rep. **37**, 1 (1999).
[30] E. Gür, G. Tabares, A. Arehart, J. M. Chauveau, A. Hierro, and S. A. Ringel, J. Appl. Phys. **112**, 123709 (2012).
[31] Y. Dong, F. Tuomisto, B. G. Svensson, A. Y. Kuznetsov, and L. J. Brillson, Phys. Rev. B **81**, 081201(R) (2010).
[32] T. M. Børseth, F. Tuomisto, J. S. Christensen, E. V. Monakhov, B. G. Svensson, and A. Y. Kuznetsov, Phys. Rev. B **77**, 045204 (2008).
[33] S. Balaz, C.-J. Ku, Y. Lu, and L.J. Brillson, "Impact of Native Defects on Electrical Characteristics of (Mg,Zn)O Thin Film Transistors" (unpublished).
[34] C.-J. Ku, Z. Duan, P. I. Reyes, Y. Lu, Y. Xu, C.-L. Hsueh, and E. Garfunkel, Appl. Phys. Lett. **98**, 123511 (2011).
[35] R. Schmidt-Grund, D. Fritsch, M. Schubert, B. Rheinländer, H. Schmidt, H. Hochmuth, M. Lorenz, C. M. Herzinger, and M. Grundmann, AIP Conf. Proc. **772**, 201 (2005).
[36] M. W. Williams and E. T. Arakawa, J. Appl. Phys. **38**, 5272 (1967).
[37] A. S. Rao and R. J. Keamey, Phys. Status Solidi B **95**, 243 (1979).
[38] T. Minemoto, T. Negami, S. Nishiwaki, H. Takakura, and Y. Hamakawa, Thin Solid Films **372**, 173 (2000).
[39] K. Jacobi, G. Zwicker, and A. Gutmann, Surf. Sci. **141**, 109 (1984).
[40] G. M. Foster, S. Mehra, J. Perkins, and L. J. Brillson, "Transient surface photovoltage spectroscopy measurements of bulk traps" (unpublished).
[41] Z. Zhang, V. Quemener, C.-H. Lin, B. G. Svensson, and L. J. Brillson, Appl. Phys. Lett. **103**, 072107 (2013).
[42] C.-.H. Lin, E. J. Katz, J. Qui, Z. Zhang, U. K. Mishra, L. Cao, and L. J. Brillson, Appl. Phys. Lett. **103**, 162106 (2013).
[43] D. A. Freedman, D. Roundy, and T. A. Arias, Phys. Rev. B **80**, 064108 (2009).
[44] C. M. Brooks, L. F. Kourkoutis, T. Heeg, J. Schubert, D. A. Muller, and D. G. Schlom, Appl. Phys. Lett. **94**, 162905 (2009).
[45] W. Windl, O. Restrepo, M. Ball, J. Perkins, G. M. Foster, M. Myer, S. Mehra, J. M. Chauveau, A. Hierro, A. Redondo-Cubero, and L. J. Brillson, "Modeling-Assisted Measurement of Chemical Potentials in $Mg_xZn_{1-x}O$" (unpublished).